Fast electrochemical deposition of $Ni(OH)_2$ precursor involving water electrolysis for fabrication of NiO thin films

Miki Koyama[1] and Masaya Ichimura[1]

[1]*Department of Electrical and Mechanical Engineering, Nagoya Institute of Technology, Gokiso, Showa, Nagoya 466-8555, Japan*

E-mail: cli13091@stn.nitech.ac.jp

ORCID: https://orcid.org/0000-0001-8904-7136

Abstract

$Ni(OH)_2$ precursor films were deposited by galvanostatic electrochemical deposition (ECD), and NiO thin films were fabricated by annealing in air. The effects of the deposition current densities were studied in a range including current densities high enough to electrolyze water and generate hydrogen bubbles. The films fabricated by ECD involving water electrolysis had higher transparency and smoother surface morphology than those deposited with lower current densities. In addition, the annealed NiO films clearly had preferred (111) orientation when the deposition was accompanied by water electrolysis. p-type conduction was confirmed for the annealed films.

1. Introduction

NiO has been extensively studied for many potential applications including solar cells [1,2], charge storage [3,4], electrochromic devices [5-7], and UV photodetector [8,9], because of the electrical, optical and chemical characteristics. Moreover, improvement of the stability of perovskite solar cells by introducing NiO as a hole transport material is

reported recently [10].

The various synthesis techniques of NiO, including physical vapor deposition [1], radio frequency sputter deposition [11], spray pyrolysis deposition [12], sol-gel deposition [13] have been reported. Electrochemical deposition (ECD) of NiO is also well-known, and both anodic [5,14] and cathodic [4,15,16] depositions have been reported. Fabrication of oxide films by ECD has excellent industrial advantages, such as inexpensiveness due to the simple equipment and capability to increase the deposition area. In the fabrication of NiO films by ECD, $Ni(OH)_2$ precursor films are first deposited, and then NiO is formed by annealing the precursor.

In most of the previous works of the cathodic ECD, nickel nitrate were used as the source material. The deposition mechanism of the $Ni(OH)_2$ precursor by reductive deposition in the aqueous nitrate solution is generally known as

$$Ni(NO_3)_2 \rightarrow Ni^{2+} + 2NO_3^- \quad (1)$$

$$NO_3^- + 2H_2O + 2e^- \rightarrow NO_2^- + 2OH^- \quad (2)$$

$$Ni^{2+} + 2OH^- \rightarrow Ni(OH)_2 \quad (3)$$

where $Ni(OH)_2$ is formed by OH^- derived from the reduction reaction of NO_3^- [17].

On the other hand, the following reactions (4)-(5) are also known as the synthesis of a metal hydroxide $M(OH)_n$ using the generation of OH^- derived from electrolysis of water [17].

$$2H_2O + 2e^- \rightarrow H_2 + 2OH^- \quad (4)$$

$$M^{n+} + n(OH)^- \rightarrow M(OH)_n \quad (5)$$

However, to our knowledge, there is no report on fabricating NiO thin films using

this mechanism. It has been generally speculated that the film surface may be roughened by the bubbles generated during water electrolysis. Therefore the potential or current generating hydrogen bubbles has been avoided in deposition of functional thin films, for which the surface flatness is essential.

In this work, $Ni(OH)_2$ precursor films are deposited by galvanostatic ECD, and NiO thin films are fabricated by annealing. The effects of the deposition current densities are studied in a range including current densities high enough to electrolyze water and generate hydrogen bubbles. Interestingly, the deposited films formed with electrolysis of water have better qualities than those deposited with lower current densities, such as higher transparency and smoother surface morphology. Details of the experiments are given in the next section, and characterization results are given in the third section.

2. Experiments

The precursor $Ni(OH)_2$ thin films were deposited electrochemically in a three-electrode cell using a Hokutodenko HA151-B potentiostat / galvanostat, with an indium tin oxide (ITO) coated glass substrate (approximately 10 Ω/cm^2) as the working electrode, an Ag/AgCl electrode as the reference electrode, and a platinum sheet as the counter electrode. The electrodeposited area was 1 cm × 1 cm. Prior to the experiment, The ITO coated grass substrate was degreased in acetone. Aqueous solutions containing 0.03 M $Ni(NO_3)_2 \cdot 6H_2O$ were used at room temperature, and the pH was not adjusted (approximately 4.4). Cathodic current densities were varied within a range from -0.4 to -8.0 mA/cm^2, and the deposition time was 60 s unless otherwise noted. NiO thin films were fabricated by heating the deposited $Ni(OH)_2$ films in air at 400 °C for 1 h after washing in ultra-pure water.

Cyclic voltammetry (CV) was conducted at a scanning rate of 20 mV/s between -3 V and 2 V with a Hokutodenko HA151-B potentiostat / galvanostat. The film thickness was measured by an Accretech Surfcom-1400D profilometer. Surface morphology of the thin films was analyzed by atomic force microscope (AFM) with Pacific nanotechnology Nano-R2 model in the noncontact mode. Raman spectra were recorded with excitation laser wavelength of 532 nm and laser power of 6.1 mW by Jasco NRS-3300 Raman spectroscopy. X-ray diffraction (XRD) patterns ($\theta/2\theta$ scan) were recorded by the SmartLab X-ray diffractometer (Rigaku) using a CuKα radiation source. The photoelectrochemical (PEC) experiment was carried out voltammetrically in a three-electrode cell with the fabricated thin films as the working electrode and a 0.1 M Na_2SO_4 aqueous solution as the electrolyte. Optical excitation of the films was done by radiating light of 100 mW/cm^2 intermittently with intervals of 5 s using an ABET technologies 10500 solar simulator, while the film was biased within a range from -1.0 to 1.0 V at a scanning rate of 5 mV/s.

3. Results

Fig. 1 shows CV for the deposition solution. In the negative potential region, a reduction peak is observed at about -1.6 V with a reduction current density of approximately -5.0 mA/cm^2. This peak corresponds to reaction (2). At less cathodic potentials (i.e. lower current densities) than this peak, reaction (2) is dominant in the deposition mechanism of $Ni(OH)_2$ thin films. At more cathodic potentials (i.e. higher current densities), electrolysis of water (reaction (4)) is dominant instead of reaction (2). In fact, at the current density of -8.0 mA/cm^2, hydrogen bubbles were vigorously generated. At low current densities (≤-4.0 mA/cm^2), hydrogen bubbles were not

observed.

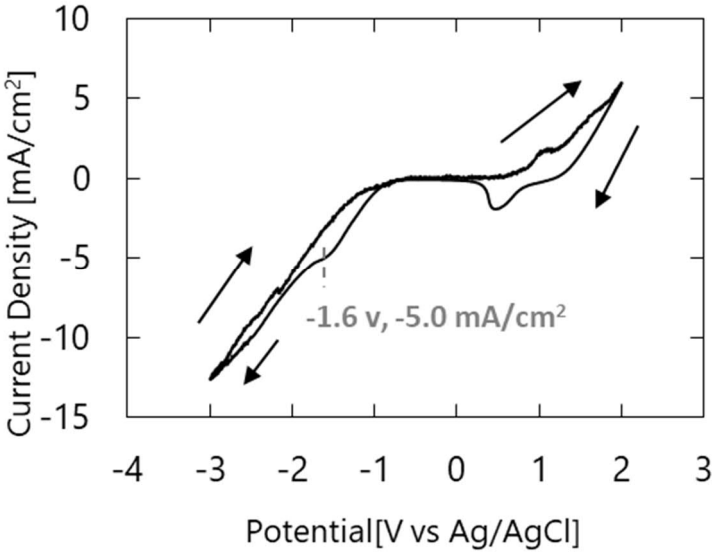

Fig. 1 Cyclic Voltammetry of the solution for $Ni(OH)_2$ deposition. The sweep rate was 20 mV/s.

Fig. 2 shows the film thickness as a function of deposition time for each current density. The thickness increases with increasing deposition time. At low current densities (≤ 4 mA), the surface becomes more rough with increasing deposition time, as shown below, and finally the films became white and cloudy. Then, the thickness profile was so rough that we could not evaluate thickness, and thus those samples are not included in Fig.2. The error bars indicate variation due to the roughness or non-uniformity of thickness. For the thick films deposited at -8.0 mA/cm^2, the surface is relatively smooth as shown below, but the thickness is larger in the bottom part of the deposition area than in the center or top part

, which results in some nonuniformity in the thickness. At low current densities (≤ -4.0 mA/cm^2), the films became highly hazy when the thickness exceeded 150-200 nm.

Thus the thickness data plotted here is only in a range of 50 - 150 nm. On the other hand, at a high current density of -8.0 mA/cm^2, the film thickness can be increased much more (up to more than 1000 nm) while surface smoothness and transparency being kept.

The theoretical values in the figure are derived from the Faraday's law of electrolysis,

$$Q = zFm \qquad (6)$$

Here, Q is the total electric charge passed through the working electrode in coulombs, z the valence of ions related to the reaction, F the Faraday constant (=96500 C mol^{-1}), and m the number of moles of electrodeposited products. The deposit was considered to be α-Ni(OH)$_2$ xH$_2$O (x = 2/3), as discussed later. The theoretical values of the film thickness T is given by

$$T = \frac{mM}{\rho S} \qquad (7)$$

Here, S is the deposition area (1 cm × 1cm), M the molecular weight, ρ the weight density of α-Ni(OH)$_2$ xH$_2$O, which was calculated using the lattice constants reported in [18]. As can be seen from the figure, for the current density of -8.0 mA/cm^2, the measured thickness agrees fairly well with the theoretical value. This indicates that the current efficiency is almost 100 %.

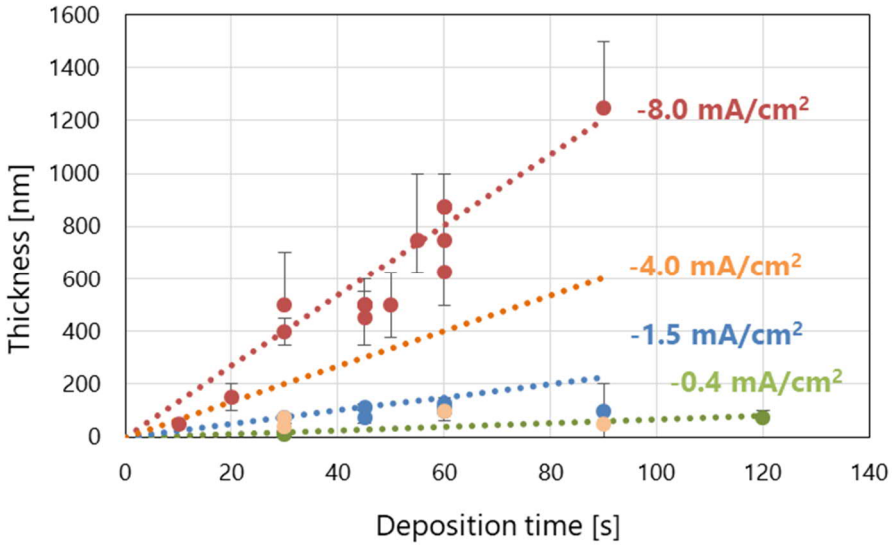

Fig. 2 Film thickness as a function of deposition time for the different current densities.

To evaluate the surface roughness quantitatively, surface morphology is analyzed with AFM for the as-deposited $Ni(OH)_2$ films. Fig. 3 shows root mean square (RMS) roughness as a function of the film thickness for the small and large deposition current densities (-1.5 and -8.0 mA/cm^2). At the current density of -1.5 mA/cm^2, where the deposition does not involve water electrolysis, RMS increases with thickness. This behavior is commonly observed in the most deposition processes. In contrast, at the current density of -8.0 mA/cm^2, where hydrogen bubbles were generated during the deposition, the surface became smoother with increasing thickness. This can also be seen in Fig.4, which shows the AFM images and the line profiles of the relatively thin and thick films deposited at those two current densities. The surface shown in Fig.4 (b) is much more rough than that in Fig.4(a), while the surface shown in Fig.4(d) is even smoother than that in Fig.4(c). The 750 nm-thick film deposited at -8.0 mA/cm^2 (Fig.4(d)) has a much smoother surface than the 150 nm-thick film deposited at -1.5

mA/cm^2 (Fig.4(b)). Accordingly, the deposition involving water electrolysis can results in deposition of much thicker films with smoother surfaces than that without water electrolysis.

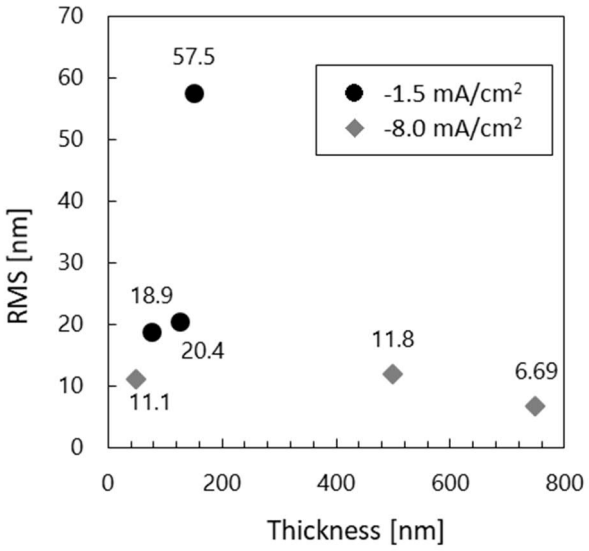

Fig. 3 Surface roughness (RMS) vs. film thickness of the as-deposited $Ni(OH)_2$ films for the two deposition current densities.

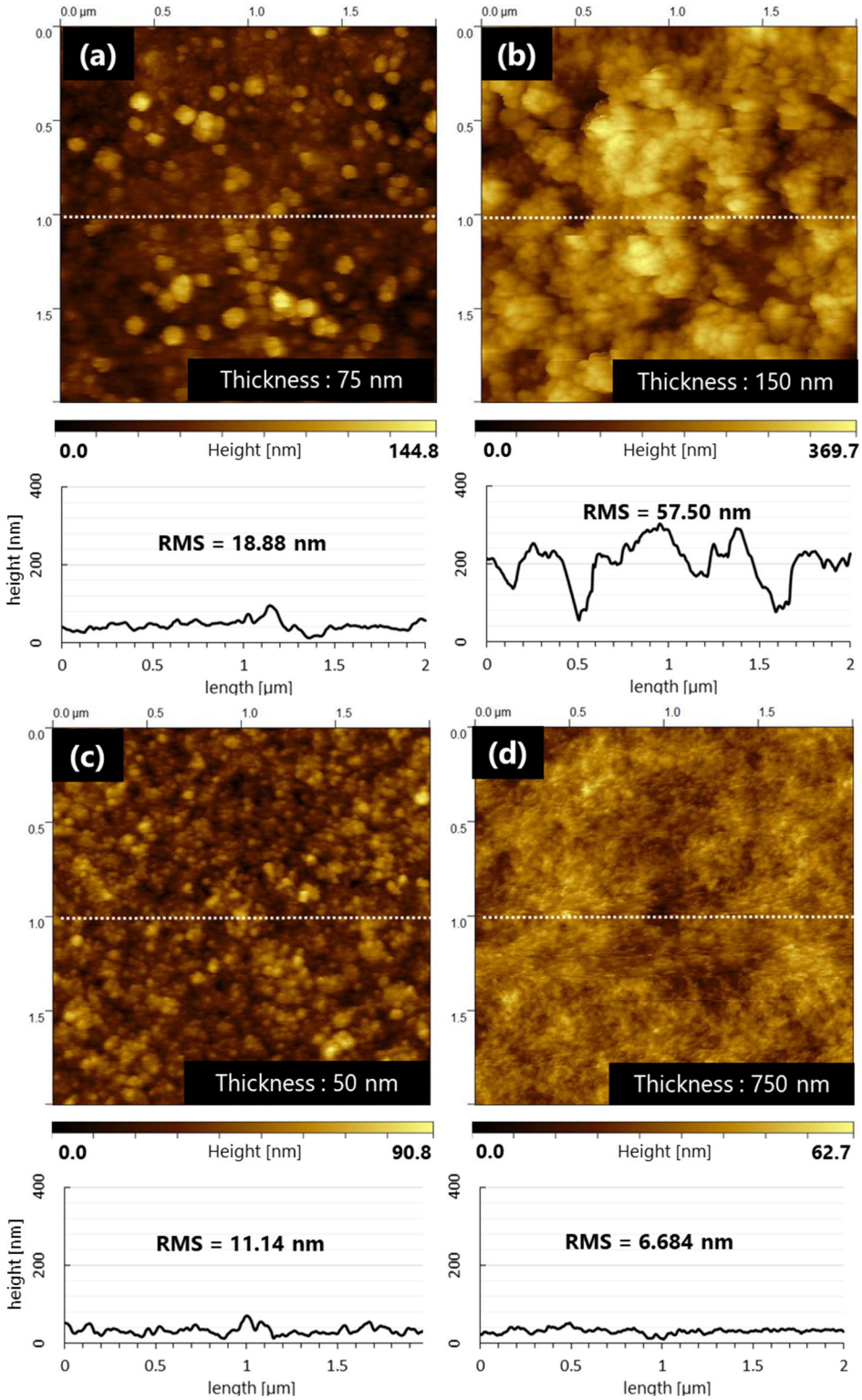

Fig. 4 AFM images and line profiles of the as-deposited $Ni(OH)_2$ films. The deposition current density and the film thickness are respectively (a) -1.5 mA/cm^2 and 75 nm, (b) -1.5 mA/cm^2 and 110 nm, (c) -8.0 mA/cm^2 and 50 nm (d)

-8.0 mA/cm^2 and 750 nm

Fig. 5 shows the Raman spectra of the as-deposited films deposited at (a) -8.0 mA/cm^2, (b) -1.5 mA/cm^2, and of the annealed films deposited at (c) -8.0 mA/cm^2, (d) -1.5 mA/cm^2. $Ni(OH)_2$ has two phases α- and β-$Ni(OH)_2$, and α-$Ni(OH)_2$ has trigonal symmetry structure consisting of planes of $Ni(OH)_2$ intercalated with water [19]. At room temperature, metastable α-$Ni(OH)_2$ can be deposited in preference to thermodynamically stable β-$Ni(OH)_2$ [18,19]. In both the spectra of the as-deposited $Ni(OH)_2$ films (a) and (b), the peaks are observed at 470, 1045, 3660 cm^{-1}. The peak at 470 cm^{-1} is thought to be derived from the lattice mode of α-$Ni(OH)_2$. The peak at 3660 cm^{-1} is derived from the O-H stretch mode. In both the spectra of the annealed NiO films (c) and (d), the peak at approximately 500 cm^{-1} is characteristic of NiO.

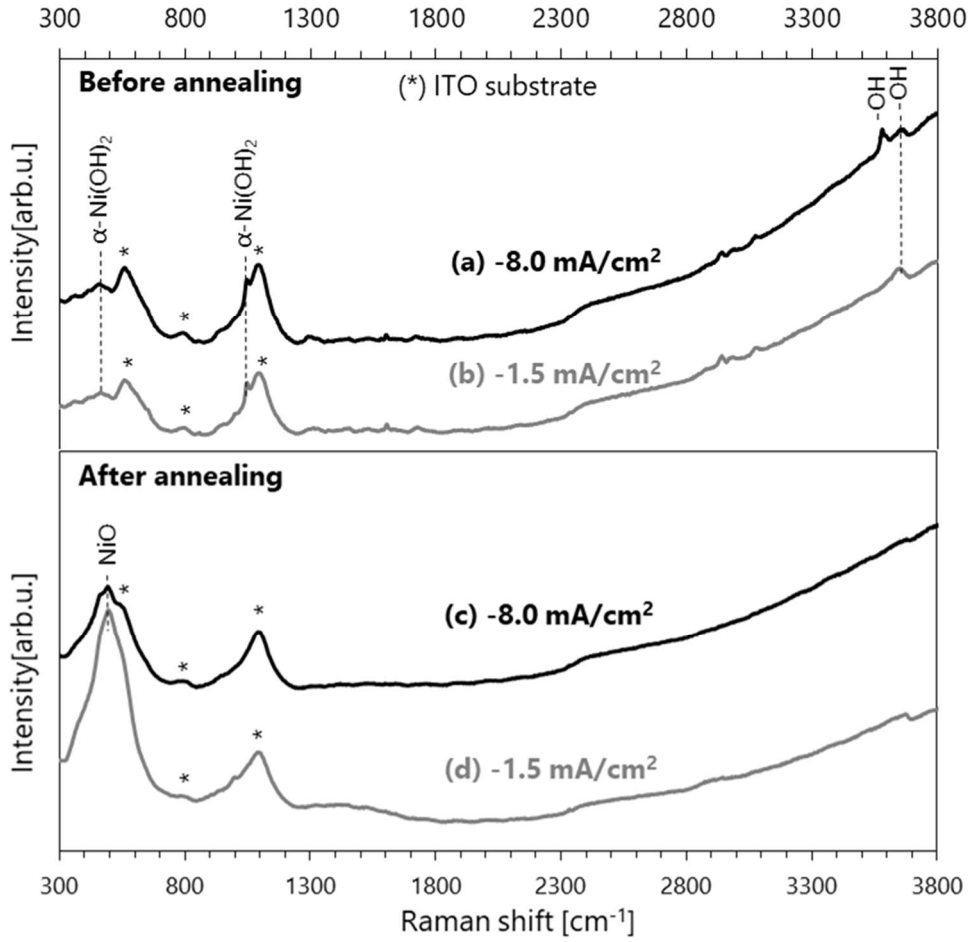

Fig. 5 Raman spectra of the as-deposited $Ni(OH)_2$ films and of the annealed NiO films for the two different deposition current densities.

Fig. 6 shows the XRD patterns of the annealed NiO films deposited at -8.0 and -1.5 mA/cm^2 with deposition time of 60 s. No peaks were observed for the as-deposited $Ni(OH)_2$ film, for all the deposition current densities. For the films deposited at -1.5 mA/cm^2, no peaks were observed even after the annealing. We observed no clear peaks either for the films deposited at low current densities at which water electrolysis was not involved. The thickness of the film deposited at -1.5 mA/cm^2 is 50 nm, smaller than that of the film deposited at -8.0 mA/cm^2 (400 nm). XRD was measured for films deposited at -1.5 mA/cm^2 with longer deposition time (up to 120 s), but no clear diffraction peaks

were observed. On the other hand, for the current density of -8.0 mA/cm^2, one peak corresponding to NiO (111) is observed clearly at 37°, and no other NiO peaks were observed. (For comparison, grazing-incidence (3º) diffraction was also measured, but no peak was observed. This is because the diffraction condition is not satisfied in the grazing mode for the oriented samples.) Thus, after the annealing, the film deposited at -8.0 mA/cm^2 with water electrolysis crystallized with strong (111) preferred orientation.

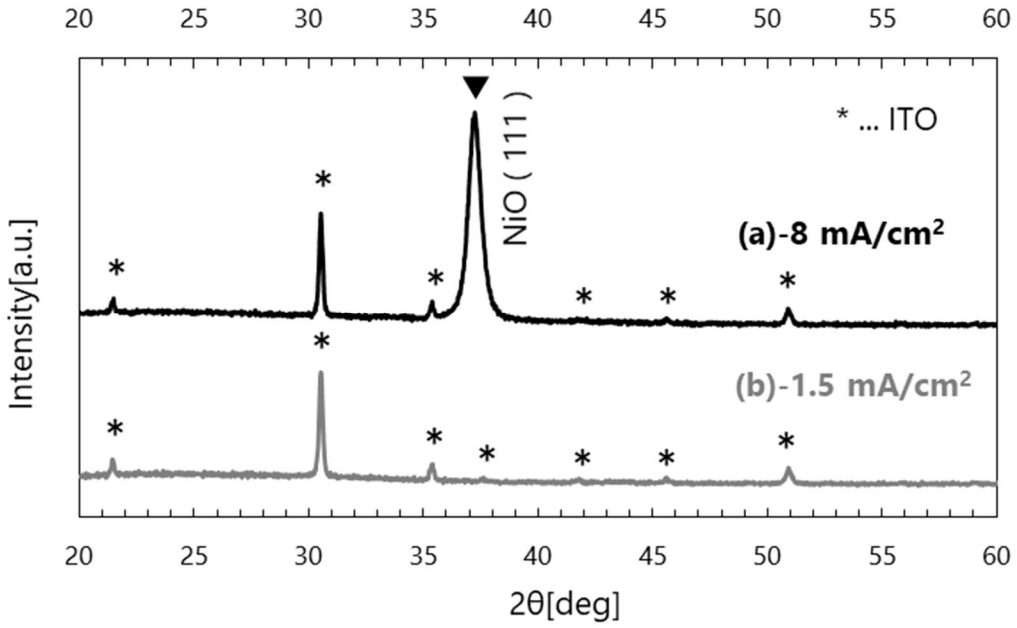

Fig. 6 XRD patterns of the annealed NiO films for the two different deposition current densities.

Fig. 7 shows the optical transmission spectra for the as-deposited $Ni(OH)_2$ films deposited at (a) -1.5 mA/cm^2 and (b) -8.0 mA/cm^2, and the annealed NiO films deposited at (c) -1.5 mA/cm^2 and (d) -8.0 mA/cm^2. Although the as-deposited $Ni(OH)_2$ films ((a) and (b)) have no absorption edge, the annealed NiO films ((c) and (d)) have the absorption edge near 370 nm. Thus, the change from an insulator to a semiconductor by the annealing was confirmed. The bandgap calculated from plot of $(\alpha h\nu)^2$ vs $h\nu$,

where α is the absorption coefficient and hν the photon energy, is 3.8 eV for (c), and 3.7 eV for (d). The thickness after the annealing is 50 nm for (c) and 400 nm for (d). Even though the thickness of the film deposited at -8.0 mA/cm^2 is much larger, the transmittance is comparable. This shows that the film deposited at -8.0 mA/cm^2 has high transparency. For the lower deposition current densities (≤ -4.0 mA/cm^2), the film became hazy and transmittance decreased significantly when the thickness exceeded 150-200 nm, as noted above.

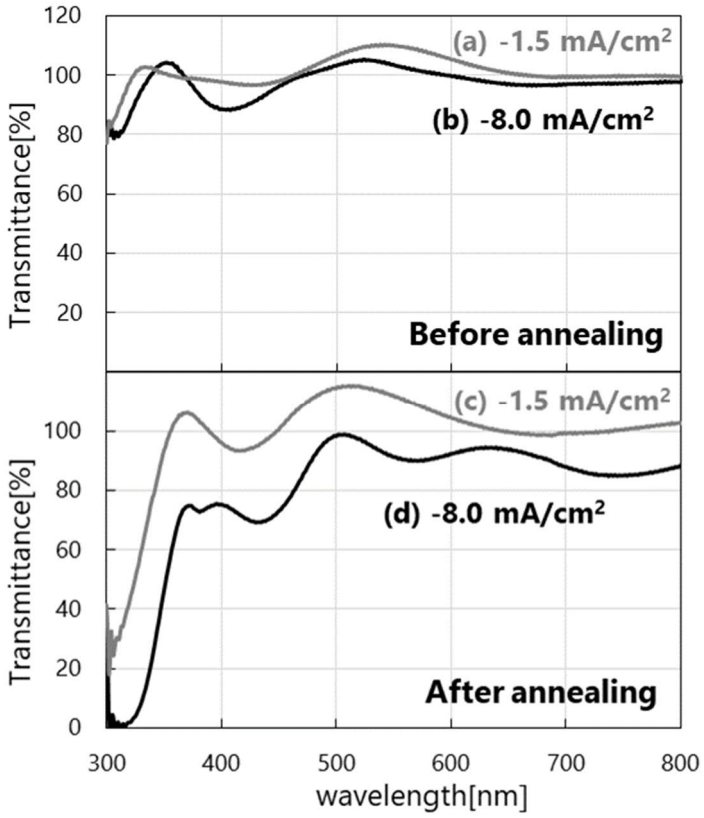

Fig. 7 Optical transmission spectra of the as-deposited $Ni(OH)_2$ films and of annealed NiO films for the two different deposition current densities.

Fig. 8 shows the PEC current density vs. potential curves for the annealed NiO films

deposited at -8.0 and -1.5 mA/cm^2. The photocurrent response was negligibly small in the anodic potential range. In the PEC measurement, photo-current due to minority carriers is dominantly observed. Therefore, the cathodic photo current evidently proves p-type character of the thin films. No photo-response was observed for the as-deposited $Ni(OH)_2$ films. Thus, insulating $Ni(OH)_2$ was converted to p-type NiO by the annealing. The films deposited under the other conditions exhibited similar photo current densities.

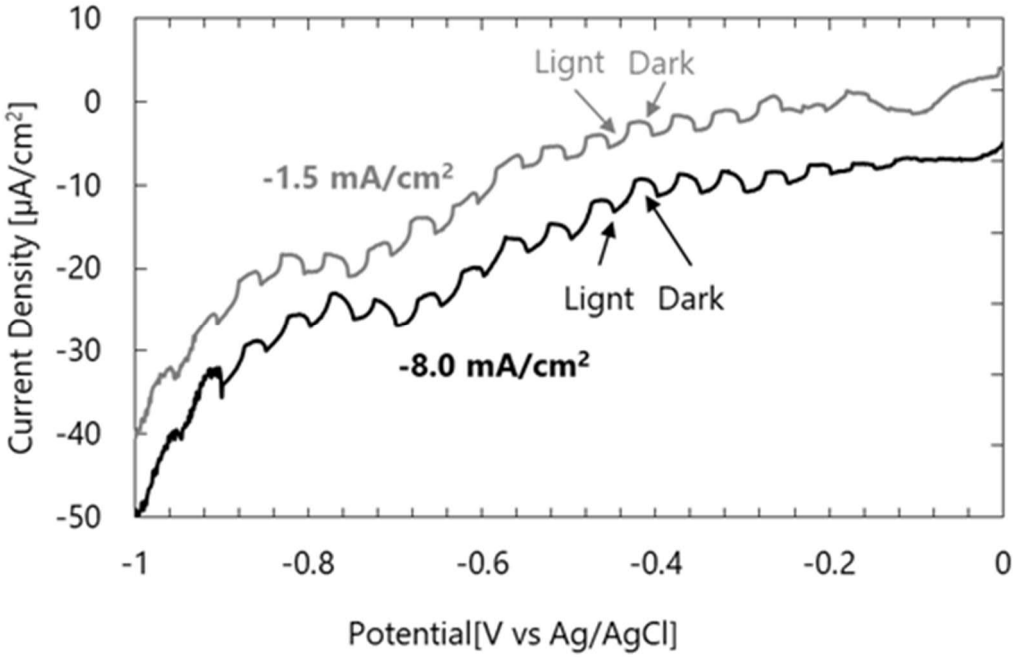

Fig. 8 Photoelectrochemical measurements of the annealed NiO films deposited at the two different deposition current densities.

4. Discussion

In the conventional deposition mechanism (2)-(3), $Ni(OH)_2$ is formed by OH^- derived from the reduction reaction of NO_3^-. On the other hand, the deposition mechanism (4)-(5) involves hydrogen-bubble generation, and $Ni(OH)_2$ is formed by OH^- derived from electrolysis of H_2O. In aqueous solutions, H_2O is most abundant, and thus the deposition

can potentially be much faster than that based on the reduction of NO_3^-. In fact, as shown in Fig. 2, for high current density of -8.0 mA/cm^2, where hydrogen bubbles were generated, the deposition rate was much higher than for lower deposition current densities with current efficiency almost equal to 100 %.

For the high current density of -8.0 mA/cm^2, the deposited films have much smoother surfaces than those deposited with lower current densities. Thus, the films can be thick (> 1000 nm), keeping high transparency. Moreover, the surface roughness even decreases with increasing thickness, as shown in Figs.3 and 4. For the lower deposition current (≤ -4.0 mA/cm^2), the film becomes hazy because of surface roughness when the thickness exceeds 150 – 200 nm. Nam et al. reported that films deposited at lower current densities were more dense and compact while films deposited at larger current densities were more porous [16]. However, they did not examine current densities high enough to cause water electrolysis. At present, we do not clearly understand why the surface becomes smooth when the deposition involves water electrolysis. One possible mechanism of the surface flattening could be softening of the film due to excess water inclusion. With high deposition rate, the deposited film may include excess water molecules and become gelled to some extent. (In fact, just after the deposition (before drying), the film was not hard but could be deformed plastically by a light scratch.) Then the roughness can be diminished owing to material flow of the deposit. After drying, the deposit is thought to lose excess water and become α-$Ni(OH)_2$ xH_2O (x = 2/3). It should also be noted that although hydrogen bubbles were actively generated during the deposition at -8.0 mA/cm^2, no traces of the bubbles are visible on the film surface. This can also be due to the softness of the film during the deposition.

After the annealing, the NiO films deposited at high current density have (111)

preferred orientation. So far, preferred orientation during growth processes has been reported for NiO, and (111) and (001) orientations were commonly observed [20-22]. The (111) surface is thought to have the lowest surface energy when the surface atomic plane is composed of oxygen atoms. In the present case, the as-deposited films are amorphous α-$Ni(OH)_2$, and the (111) orientation takes place during the annealing, not the deposition. During the annealing in air, α-$Ni(OH)_2$ is thought to gradually lose water and crystallize to become NiO. This process would probably begin at the surface. Since the surface of the film deposited at -8.0 mA/cm^2 is fairly smooth, a flat (111) plane composed of oxygen atoms can be formed on the surface. Then the crystallization can proceed from the surface to the bulk with preferred (111) orientation.

Thus, we conclude that ECD involving water electrolysis, which had been avoided conventionally, is in fact advantageous for fabricating NiO thin film devices such as solar cells and sensors, for which roughness of the surface and interface must be minimized. Furthermore, ECD involving water electrolysis may also be able to be applied to other various functional metal hydroxide and oxide thin films.

5. Conclusions

In this work, $Ni(OH)_2$ thin films were electrodeposited from aqueous 0.03 M nickel nitrate electrolytes galvanostatically at cathodic deposition current densities within a range from -0.4 to -8.0 mA/cm^2. It was discovered that the films deposited at -8.0 mA/cm^2 with electrolysis of water was drastically thicker with higher transparency and less surface roughness than those deposited at lower current densities. By annealing at 400 °C, transparent p-type NiO films with (111) orientation were obtained. Thus, electrodeposition involving electrolysis of water is advantageous for fabrication of

optoelectronic devices based on NiO.

List of references

1. H. Ohta, M. hirano, K. Nakahara, H. Maruta, T. Tanabe, M. Kamiya, T. Kamiya, H. Hosono, Appl. Phys. Lett. 83, 1029 (2003)
2. R. Karsthof, P. Ra¨cke, H. von Wenckstern, M. Grundmann, Phys. Status Solidi, A 213, 30 (2016)
3. K. C. Liu, M. A. Anderson, J. Electrochem. Soc. 143, 124 (1996)
4. V. Srinivasan and J. W. Weidner, J. Electrochem. Soc. 144, L210 (1997)
5. C. Natarajan, H. Matsumoto, G. Nogami, J. Electrochem. Soc. 144, 121 (1997)
6. A. C. Sonavane, A. I. Inamdar, P. S. Shinde, H. P. Deshmukh, R. S. Patil, P. S. Patil, J. Alloy. Comp. 489, 667 (2010)
7. F.F. Ferreira, M.H. Tabacniks, M.C.A. Fantini, I.C. Faria and A. Gorenstein, Solid State Ionics, 86-88, 971 (1996)
8. D. Y. Kim, J. Ryu, J. Manders, J. Lee, F. So, Appl. Mater. Interfaces, 6, 1370 (2014)
9. M. R. Hasan, T. Xie, S. C. Barron, G. Liu, N. V. Nguyen, A. Motayed, M. V. Rao, R. Debnath, Appl. Mater. 3, 106101 (2015)
10. M. Yanagida, L. Shimomoto, Y. Shirai, K. Miyano, Electrochemistry, 85, 231 (2017)
11. J. S. E. M. Svensson, C. G. Granqvist, Appl. Phys. Lett. 49, 1566 (1986)
12. P. S Patil, L.D. Kadam, Appl. Surf. Science. 199, 211 (2002)
13. E. O. Zayim, I. Turhan, F. Z. Tepehan, N. Ozer, Sol. Energ. Mater. 92, 164–169 (2008)
14. K. Nakaoka, J. Ueyama, K. Ogura, J. Electroanal. Chem. 571, 93 (2004)
15. F. Vera, R. Schrebler, E. Mun˜oz, C. Suarez, P. Cury, H. Go´mez, R. Co´rdova, R.E.

Marotti, E.A. Dalchiele, Thin Solid Films 490, 182 (2005)

16. K. Nam, K. Kim, J. Electrochem. Soc. 149, 346 (2002)
17. G. H. A. Therese, P. V. Kamath, Chem. Mater, 12, 1195 (2000)
18. D. S. Hall, D. J. Lockwood, C. Bock, B. R. MacDougall, Proc. R. Soc. A471, 10 (2014)
19. D. S. Hall, D. J. Lockwood, C. Bock, S. Poirier, B. R. MacDougall, J. Phys. Chem. A, 116, 6771 (2012)
20. H.-L. Chen, Y.-M. Lu, W.-S. Hwang, Mater. Trans., 46, 872 (2005)
21. B.A. Reguig, M. Regragui, M. Morsli, A. Khelil, M. Addou, J.C. Berne`de, Sol. Energy Mater. Sol. Cells 90, 1381 (2006)
22. J.-K. Kang, S.-W. Rhee, Thin Solid Films 391, 57 (2001)